International Journal of Design & Nature and Ecodynamics
Vol. 20, No. 4, April, 2025, pp. 945-955
Journal homepage: http://iieta.org/journals/ijdne

Green Synthesis of Iron Nanoparticles Using Gum Arabic (*Acacia senegal*): Antimicrobial, Anticoagulant, and Wound-Healing Applications

Ashwaq T. Hameed[1*], Estbrak Y. Ashoor[1], Nabaa Q. Jameel[1], Noora H. Ibrahim[2]

[1] Department of Biology, College of Education for Women, University of Anbar, Ramadi 31001, Iraq
[2] University Headquarter Department, University of Anbar, Ramadi 31001, Iraq

Corresponding Author Email: ashwaq.talib@uoanbar.edu.iq

https://doi.org/10.18280/ijdne.200423

Received: 3 March 2025
Revised: 8 April 2025
Accepted: 22 April 2025
Available online: 30 April 2025

Keywords:
FeNPs, biofilm inhibition, wound healing, coagulation, antibacterial, gum Arabic

ABSTRACT

Recently, iron nanoparticles (FeNPs) synthesized using gum arabic as a green reducing agent have demonstrated significant biological activity, highlighting the potential of nanotechnology in biomedical applications. The FeNPs were prepared by dissolving 4.04 g of iron nitrate [$Fe(NO_3)_3$•$9H_2O$] in 100 mL of deionized water, heating the solution to 60°C for 1 hour, and then mixing it with 10 mL of plant extract. The color of the solution turned reddish brown, confirming the formation of nanoparticles. The biocompatibility of FeNPs, along with their antimicrobial, anticoagulant, and wound-healing activities, suggests their potential applications in healthcare. The antimicrobial properties of FeNPs were evaluated against several bacterial strains, including *Staphylococcus aureus*, *Staphylococcus epidermidis*, *Escherichia coli*, and *Pseudomonas aeruginosa*. The results showed that the nanocomposite exhibited significant inhibitory effects against *Staphylococcus* species, with inhibition rates ranging from 61.96% to 77.82% across various concentrations. These findings suggest that FeNPs inhibited biofilm formation in Staphylococcus species, which were the most sensitive bacteria tested, in a concentration-dependent manner. This suggests that FeNPs could serve as a suitable replacement for conventional antibacterial substances, especially for infections that involve biofilms. The anticoagulant activity of FeNPs was assessed by measuring prothrombin time (PT) and partial thromboplastin time (PTT) at concentrations ranging from 50 to 100 µg/mL. A marked increase in clotting time was observed, indicating strong anticoagulant effects. The greatest delay in clotting was observed at the concentration of 100 µg/mL. This effect is attributed to the interaction of FeNPs with key coagulation factors (VIII, IX, and XI), which delays thrombin formation and alters fibrin production. Additionally, Fe NPs generate reactive oxygen species (ROS) that influence platelet activity, further aiding in the prevention of blood clots. FeNPs were shown to accelerate fibroblast migration and collagen synthesis during the wound healing process. The treated group exhibited a significantly higher rate of scratch closure (~88%) compared to the untreated group (~78%) after 72 hours. FeNPs were shown to accelerate fibroblast migration and collagen synthesis during the wound healing process. The treated group exhibited a significantly higher rate of scratch closure (~88%) compared to the untreated group (~78%) after 72 hours. Moreover, these particles are also capable of inducing angiogenesis and activating the immune system. The gum Arabic-synthesized Fe NPs exhibited strong antimicrobial, anticoagulant, and wound-healing activities, demonstrating their high potential in biomedical applications. Further studies are required to optimize their efficacy and safety for use in patient care settings.

1. INTRODUCTION

Iron nanoparticles (FeNPs), among the many nanomaterials currently under investigation, have garnered significant attention due to their unique physicochemical properties, such as high surface area and enhanced reactivity, which render them highly effective in various applications [1, 2]. Recent studies have highlighted the potential of FeNPs synthesized from natural sources such as gum arabic (*Acacia senegal*) [3]. Their remarkable bioactivity is attributed to the presence of various bioactive constituents, particularly phenolic compounds, glycosides, and β-D-galactopyranosyl groups [4]. Despite the potent antibacterial, anticoagulant, and wound-healing properties of FeNPs, antibiotic resistance remains one of the greatest challenges in modern medicine, rendering many conventional treatments ineffective against pathogenic bacteria [5, 6]. In this context, iron oxide nanoparticles (FeONPs) synthesized through eco-friendly methods have emerged as viable candidates for biomedical applications [7, 8]. The use of non-toxic and inexpensive plant extracts enables precise control over nanoparticle size, morphology, and surface characteristics, thereby enhancing their therapeutic

efficacy [9, 10]. For instance, the antibacterial activity of surface-modified FeONPs can be enhanced by coating them with polyindole carboxylates, which facilitate binding to bacterial proteins and effectively inhibit microbial growth [11]. A notable example includes the use of plant extracts from species such as *Allium eriophyllum* Boiss., which exhibit strong antioxidant, antibacterial, antifungal, and anti-cytotoxic properties. These nanoparticles promote wound healing by stimulating fibroblast proliferation, reducing inflammatory markers, and mitigating microbial infections at wound sites, owing to their potent antibacterial properties [12, 13]. Furthermore, they contribute to tissue repair by stimulating collagen synthesis, thereby improving the strength and elasticity of regenerated tissue, and by activating immune cells to accelerate wound closure [14]. Innovative approaches, such as integrating iron oxide nanoparticles with lactic acid bacteria into electrospun wound dressings, have demonstrated significant antibiotic activity and excellent compatibility with fibroblasts, further underscoring their potential in biomedical applications [15, 16]. The hybridization of bioactive compounds with iron oxide nanoparticles (FeNPs) enables their application as multifunctional agents, including wound healing, antibacterial, and anticoagulant therapies. Additionally, FeNPs have demonstrated remarkable anti-inflammatory, antioxidant, and antimicrobial efficacies—reaching up to 91% in certain assays—and have shown effectiveness in controlling thrombus formation and enhancing wound healing in mouse fibroblast cells [17, 18]. The production of reactive oxygen species (ROS) and the breakdown of the bacterial cell wall are the main mechanisms behind their actions that together inhibit bacterial growth [19]. They also stimulate angiogenesis, activate fibroblasts, and aid in tissue repair [20]. By interacting with important components, including factor VIII and IX, they accelerate the wound healing process [21, 22]. This study aims to evaluate the properties of iron nanoparticles prepared using the green method from gum arabic as anti-biofilm, anticoagulant, and wound-healing agents. Specifically, the study investigates their ability to inhibit bacterial growth, delay coagulation (as measured by PT and PTT), and promote wound healing.

2. Materials and Methods

2.1 Preparation of gum Arabic extract

Gum arabic was purchased from a Shanghai company in China, and 50g of it was dissolved in 250 mL of deionized water. The solution was then heated to 60℃ and held at this temperature for 1 hour. This extract was then used in the synthesis of iron oxide nanoparticles by gradually mixing it with an iron nitrate solution.

2.2 Synthesis of iron oxide nanoparticles

4.04g of 99.99% original iron nitrate ($Fe(NO_3)_3 \cdot 9H_2O$) from Sigma-Aldrich (India) were dissolved in 100ml of deionized water to create iron oxide nanoparticles. After being heated to 60℃, the solution was kept there for an hour. The combination was then progressively mixed with 10 mL of a plant extract solution, which caused the solution to turn reddish-brown. Seeing this slow hue shift verified that nanoparticles were forming. Iron ions undergo reduction and oxidation during the manufacturing process when they interact with the plant extract's bioactive ingredients, which include flavonoids and polyphenols. These biomolecules, rich in electrons and functional groups (-OH), efficiently reduce iron ions (Fe^{2+} or Fe^{3+}) to metallic iron (FeO). Once stabilized, the iron oxide nanoparticles are ready for use [23].

2.3 Characterization of iron oxide nanoparticles

1. X-ray diffraction (XRD)

The crystal structure of the biosynthesized iron oxide nanoparticles was analyzed using XRD. A CuKα radiation source (wavelength λ = 1.54 Å) was used for this purpose. The powdered sample was scanned in the range of 20° to 70° at an angle of 2θ, with an operating current of 30 mA and a voltage of 40 kV. The diffraction pattern was recorded, and the average crystallite size of the nanoparticles was calculated using the Debye-Scherrer equation:

$$D = \frac{k\lambda}{\beta \cos \theta}$$

where, D is the crystallite size, k is the shape factor (0.94), λ is the X-ray wavelength (1.5418 Å), β is the full width at half maximum (FWHM) in radians, and θ is the Bragg angle.

2. Scanning electron microscopy (SEM)

The shape and structure of the synthesized nanoparticles were analyzed using a SEM, model MIRA3-FRENCH. Prior to imaging, the samples were dehydrated and secured onto conductive adhesive tape fixed to a specimen holder. To improve electrical conductivity, a thin platinum-gold coating was applied via sputtering. SEM imaging was performed at an acceleration voltage of 80 kV [24].

3. Atomic force microscopy (AFM)

The size, dispersion, and surface properties of the nanoparticles were evaluated using a high-resolution Angstrom AA2000 AFM. To prepare the sample, a droplet of the nanoparticle suspension was deposited onto a 1 cm^2 glass substrate and air-dried before analysis. All AFM measurements were performed at ambient temperature and pressure..

4. Fourier-transform infrared spectroscopy (FTIR)

Infrared spectroscopy was used to identify the functional groups on the surface of the nanoparticles. A Shimadzu-8400 spectrometer, operating in the wavenumber range of 50 to 5000 cm^1, was used to conduct the measurements. For accurate analysis, the instrument combines FTIR spectroscopy with an optical microscope.

5. UV-Visible spectroscopy

Using UV-Vis spectroscopy to study the formation of iron oxide nanoparticles. By observing the surface plasmon resonance (SPR) band at the wavelength of 300-700 nm, to prove the success of the synthesis of nanoparticles.

2.4 Effect of iron nanoparticles on pathogenic wound isolates

Pathogenic bacterial samples were isolated from the microbiology laboratories of Ramadi Teaching Hospital in Iraq, such as *Staph. aureus, Staph. epidermidis, E. coli and P. aeruginosa*. In September 2024, wound infections of different

origins resulted in these bacterial cultures, which were validated by the laboratory staff. The biofilm formation of these cultures was attempted to be evaluated in an educational manner using iron nanoparticles at concentrations of 25, 50, and 100 mg/mL [25].

2.5 Effect of iron nanoparticles on blood coagulation factors

Blood samples were obtained from five healthy individuals aged 20-40 years without any history of coagulation disorders. The samples were centrifuged at 2000 rpm for 15 minutes to separate plasma from the red blood cells, white blood cells, and platelets. The supernatant was then treated with iron nanoparticles at the concentrations of 2, 4, 6, 8, 10, 50, and 100 mg/mL in a 1:1 ratio. The mixtures were adjusted to 37℃ for 5 minutes without shaking. Control samples with no nanoparticles were also prepared [26]. In a glass tube, 100 microliters of plasma treated with nanoparticles were mixed with 200 microliters of PT reagent. The mixture was incubated at 37℃ for 5 minutes, and the clotting time was measured in seconds using a timer. This procedure was repeated for all nanoparticle concentrations and samples. The PTT test evaluates the intrinsic coagulation pathway. In a glass tube, 100 microliters of plasma treated with nanoparticles were mixed with 100 microliters of PTT reagent and incubated at 37℃ for 5 minutes. The anticoagulant Ethylene Diamine Tetra Acetic Acid (EDTA) was used as a control. The clotting time was measured in seconds, and the procedure was repeated for all concentrations and samples [27].

2.6 Statistical analysis

The data were expressed as mean ± standard error. Statistical comparisons between means were performed with one-way ANOVA, supplemented by LSD (least significant difference) and Tukey's post hoc tests. A P-value below 0.05 was considered statistically significant for all analyses. The statistical evaluations were carried out using SPSS software (version 17).

3. RESULTS AND DISCUSSION

3.1 XRD analysis and SEM

The XRD technique was used to determine the phase identity, purity, and structure of FeNPs synthesized using the eco-friendly method in Figure 1(A). X-ray diffraction (XRD) was used to confirm the crystalline nature and purity of FeNPs, and characteristic diffraction peaks were observed at different 1θ values, namely 10.12°, 22.02°, 22.05°, and 22.06° for 1M FeNPs. The diffraction peaks were observed for a solution containing a 25 mM concentration of FeNPs. The presence of diffraction peaks of FeNPs at characteristic angles, along with their corresponding Miller indices, was confirmed as shown in Figure 1. The expected average diameters of FeNPs nanoparticles synthesized using eco-friendly techniques at 25 mM and 1 mM concentrations were 3nm and 5nm, respectively. The fraction 9 out of 16 is equivalent to the decimal value 3.3. This analysis is correlated with XRD.

Using a SEM, we analyzed the surface morphology and size of the eco-friendly synthesized FeNPs and presented them in Figure 1(B). The SEM image clearly indicates that the shape of the synthesized iron nanoparticles is rod-shaped. Furthermore, the shapes and average crystal sizes of the FeNPs were determined to be mostly spherical or non-spherical. The average dissociative cupping duration reported from SEM and XRD analysis (40 and 20cm for different concentrations) shows almost perfect consistency, as shown in Figure 1.

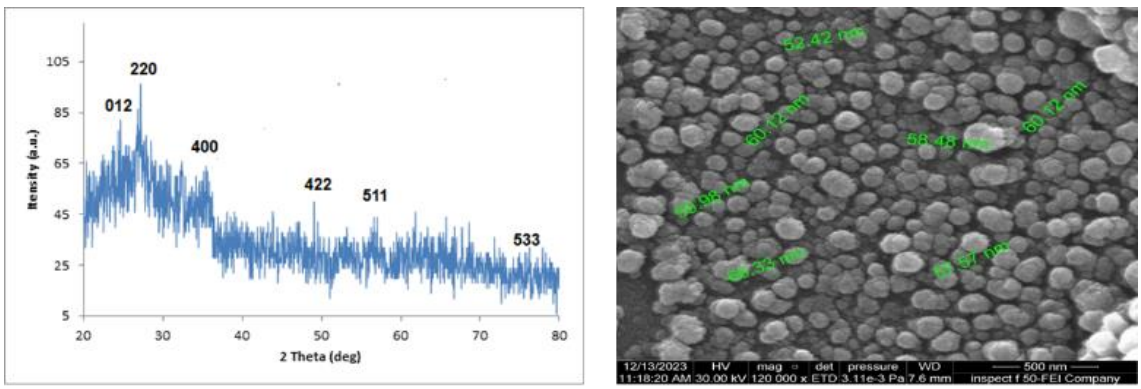

Figure 1. (A) XRD analysis of FeNPs, (B) SEM

3.2 AFM

Figure 2 shows the AFM tolerance ratio analysis and illustrates the surface morphology of the biosynthesized green iron nanoparticles. The two-dimensional AFM height plot reveals a relatively uniform striped texture, showing that the different iron nanoparticles synthesized lie within a small range, with significant variation at lower average diameters (possibly less than 50 coulombs). This indicates a robust air volume distribution, which is particularly desirable for applications. A three-dimensional topographic view of the colored graphs of the iron nanoparticles, representing capillaries and nanometers (nm), up to about 5000 coulombs, is also shown. The z-axis (height) is also represented in nanometers (nm), with a colored bar on white indicating the height scale, which runs from 0 (red) to about 97.54 coulombs (blue). It appears granular and uneven, a characteristic of a dispersed, independent deposit on a substrate. The contrasting colors on the surface indicate differences in height, making their size an independent interval and any clumps. The presence of different features (green, blue, and black) indicates larger particles or clusters, which helps with the observed tail in the histogram. The air analysis indicates that the green method used resulted in mostly small iron nanoparticles with

a narrow size distribution. However, there is an increase in the histogram for longer specifications in the three-dimensional surface view, indicating the presence of some larger air clumps. The gradual shift of the red curve indicates a moderate difference in surface roughness. The AFM results indicate that the green synthesis method used to produce iron nanoparticles resulted in primarily small nanoparticles with a relatively homogeneous size distribution. Obtaining nanoparticles with a small and uniform size is desirable for many applications due to the strong relationship between particle size and their physical and chemical properties.

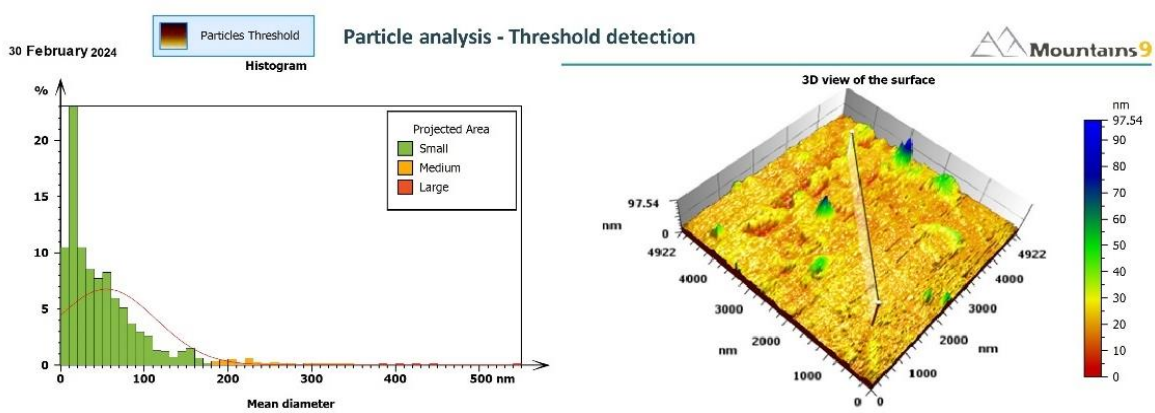

Figure 2. AFM

3.3 FTIR

Figure 3 shows the Fourier transform infrared spectra of the reduced iron oxide solution with gum Arabic extract after several weeks to identify the active components that reduced the material and dissolved it into nanoparticles. A broad band was visible around 3265.53 cm^{-1}. This broad, prominent absorption band is characterized by oxygen-hydrogen stretching vibrations. This may arise from the hydroxyl groups of alcohols, phenols, or carboxylic acids present in the gum Arabic extract. It can also be attributed to adsorbed water molecules. The broadening of the peak indicates the presence of hydrogen bonding, which is common for these types of functional groups. This presence indicates the presence of a hydrophilic component within the extract that can interact with the aqueous environment surrounding the nano iron. This could stem from the alcohol, phenolic, or carboxylic hydroxyl moieties within the gum Arabic extract. Moreover, it may come from water molecules bound to the material. The peak broadening reveals the existence of hydrogen bonding, which is typical for such functional groups. This indicates the sap, alongside other components within the extract, contains hydrophilic elements that possess the ability to interact with the surrounding media comprising water in the vicinity of the nano iron. A peak is seen at 2925.87 cm^{-1}. The peak also lies within the region typically associated with the carbon-hydrogen stretching vibrations in aliphatic groups (CH_2, CH_3), demonstrating the presence of hydrocarbon chains in the extract, thus suggesting further the presence of hydrophobic constituents which may contribute to the stabilization or the interaction of iron nanoparticles with nonpolar media.

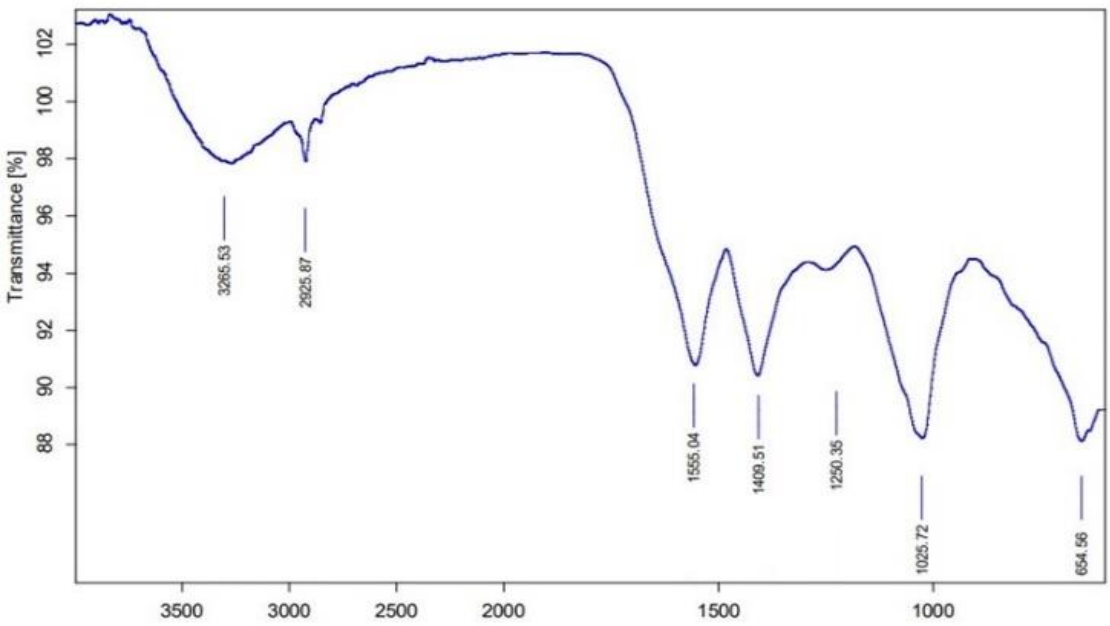

Figure 3. FTIR analysis of FeNPs

Most notably, the peak at 1555.04 cm^{-1} is interesting and can be attributed to many other possibilities. N-H bending vibrations for some of the primary or secondary amines and or the derivatives: Plant extracts are able to be associated from compounds containing nitrogen; C=C stretching vibrations in the aromatic rings: This suggests the existence of some aromatic compounds in the extract; and the asymmetric stretch of carboxylic ions (COO^-) bond. Also, if the carboxylic acids in the extract are deprotonated and coordinated with iron. The peak at 1409.51 cm^{-1} is likely due to C-H bending vibrations of CH_2 or CH_3 groups. It also supports the presence of aliphatic components. It is also likely to represent symmetric stretching of carboxyl ions (COO^-), especially if the peak at 1555.04 cm^{-1} results from asymmetric stretching. The presence of both symmetric and asymmetric carboxyl stretches strongly suggests coordination of carboxyl groups to iron nanoparticles. The peak at 1250.35 cm^{-1} is often associated with C–O stretching vibrations, especially in phenols, carboxylic acids, or esters. If this peak is shifted compared to the pure extract, it may indicate the involvement of these functional groups in binding to nano-iron. The peak at 1025.72 cm^{-1} can be attributed to C–O bond stretching in alcohols or ethers, or possibly C–N bond stretching in amines. Polysaccharides, common in plant gums, also show absorption in this region due to C-O-C bond stretching. These types of functional groups can contribute to the steric stability of nanoparticles. Peak at 654.56 cm^{-1}: This low-frequency peak is of particular interest in the context of nano iron. It is likely attributable to iron oxide (Fe-O) bond stretching vibrations. The presence of a peak in this region, especially if absent in the spectrum of the pure plant extract, strongly suggests the formation of iron oxide nanoparticles or the coordination of oxygen-containing functional groups from the extract to the iron surface. This provides direct evidence of an interaction between the extract and iron at the molecular level. Polysaccharides highlighted by the peak at 1098 cm^{-1}, as well as other hydrophilic molecules, can serve as surfactants because they lower the surface tension of the medium and help in the emulsification and dispersion of the iron nanoparticles. This illustrates the existence of iron oxide or organo-iron complexes that are believed to exist due to the bonding of the nano iron's functional groups and the plant extract's functional groups.

3.4 UV-Visible spectroscopy

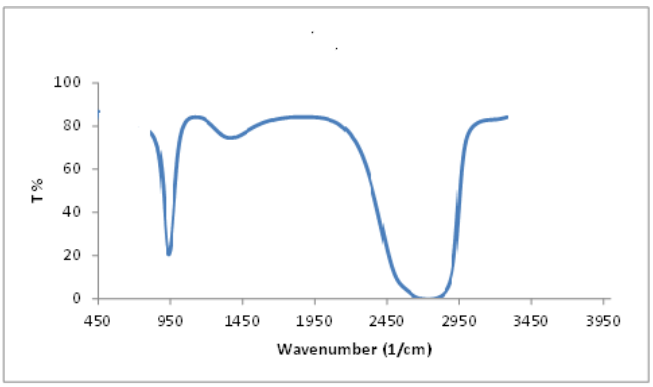

Figure 4. UV-Visible spectroscopy of FeNPs

To study the formation and stability of reduced iron nanoparticles in colloidal solution, the UV-Vis spectrometer shown in Figure 4 was used. The iron nanoparticles had surface plasmon resonance (SPR) at wavelengths of 450 and 420 nm. This indicates that they absorbed the lightest in the UV-visible range. Surface Plasmon Resonance (SPR) patterns are commonly used as diagnostic techniques to detect the formation of metal nanoparticles. The SPR phenomenon is influenced by various parameters, such as the nanoparticle size and the dielectric constant of the surrounding medium. The process of reducing Fe ions outside the cell took place, indicating the formation of silver nanoparticles (Figure 4).

3.5 The effect of nano-iron on the ability to form the biofilm

The results are shown in Table 1 and Figure 5 by using the micro-titration plates method (MIP), which is considered the easiest and most accurate method, where a large number of isolates that produce biomembrane can be obtained, this test can be validated as a quantitative analysis because it gives a digital value for the absorbance at a wavelength of 630 nanometers to detect the ability of isolates to form biomembranes using an ELISA READER) to find out the amount of biomembrane formed by adhesions on the surface according to the measurement that the thickness of the biomembrane formed before isolation is represented by absorbency [28, 29], the results showed that the bacterial isolates had the ability to produce biomembrane in different proportions in the experiment and gave different readings depending on the absorbency of the isolates as shown in Table 1, that The decrease in absorbance value of bacterial isolates after treatment with nano-iron, the ability to inhibit the adhesion of bacteria in the hole in the calibration table.

Table 1. The effect of FeNPs on the Inhibition of membrane formation %

Bacteria Isolates	Concentration (mg/mL)		
	25	50	100
Staph. aureus	61.96± 0.31	61.96± 1.25	50.3± 0.34
Staph. epidermidis	77.82± 0.03	75.89± 0.16	73.3± 0.29
E. coli	63.89± 0.25	63.54± 0.81	60.45± 0.24
P. aeruginosa	58.29± 0.03	46.89± 0.22	43.92± 0.54
LSD5%		2.034	

Results represent (mean ± SD)

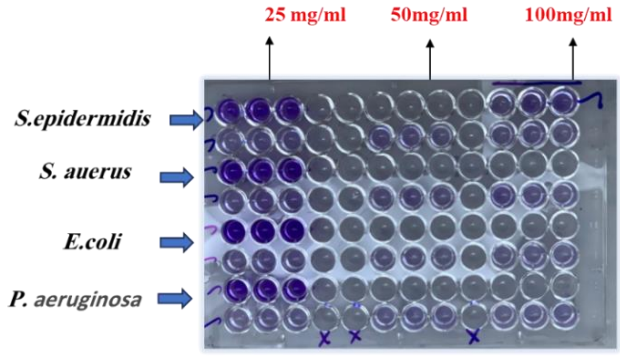

Figure 5. Biofilm formation by wound bacterial isolates using FeNPs

The results demonstrated the inhibitory effect of nano-iron on biofilm formation through an Arabic gum-derived nanocomposite at various concentrations (25, 50, and 100 mg/mL) against four bacterial isolates, *Staph. aureus*, *Staph. epidermidis*, *E. coli*, and *P. aeruginosa*, the nanocomposite exhibited varying levels of efficacy against the tested bacterial

isolates. Nano-iron showed relatively high inhibition rates against *Staphylococcus* species, with values ranging from 61.96% to 77.82% at different concentrations, indicating its potential as an antimicrobial agent against these bacteria. The inhibition rate against *E. coli* was moderate, ranging from 60.45% to 63.89%, while nano-iron exhibited the lowest inhibition against *P. aeruginosa*, with values ranging from 43.92% to 58.29%. This suggests that the nanocomposite may be less effective against *P. aeruginosa*.

Notably, the inhibition rate generally increased with higher nanocomposite concentrations, indicating a dose-dependent effect. However, the magnitude of this increase varied among different bacterial isolates. The presented data cover only four bacterial isolates; therefore, further research is required to assess the efficacy of the nanocomposite against a broader range of bacterial species. Numerous studies have explored the antimicrobial properties of Arabic gum as a nanomaterial precursor. Study [30] indicated that bacterial isolates possess the ability to form biofilms, a capability influenced by environmental conditions such as temperature, pH, and nutrient availability. This ability is attributed to the abundance of molecules secreted by bacteria to adhere to the extracellular matrix [31].

The impact of nano-iron on pathogenic bacterial biofilms varies significantly based on nanoparticle size, concentration, surface modifications, and application methods. Small nanoparticles (2 nm) have been reported to enhance biofilm formation in P. aeruginosa by increasing the bioavailability of dissolved iron, thereby promoting bacterial growth. Additionally, these small nanoparticles weaken host antimicrobial peptides, such as lysozyme, through surface adsorption [32]. In contrast, larger nanoparticles (43-540 nm) exhibit reduced interference with bacterial growth and antimicrobial peptide function compared to smaller particles [33]. Higher concentrations (0.15 mg/mL) of iron oxide nanoparticles have been found to reduce biofilms by inducing oxidative stress through reactive oxygen species (ROS), physically disrupting cell membranes via electrostatic interactions, and damaging bacterial proteins and DNA. These effects have resulted in inhibition zones of up to 29 mm [34]. Conversely, lower concentrations (≤0.1 mg/mL) demonstrate minimal or no anti-biofilm effects. Polymer-coated surfaces combined with iron oxide nanoparticles have been shown to reduce bacterial adhesion by 80% and biofilm growth by 50% compared to uncoated surfaces [35]. Hyperthermia applications utilizing magnetic iron oxide nanoparticles have also demonstrated biofilm dispersion and enhanced antibiotic efficacy by generating localized heat (43-60℃) under magnetic fields. This approach has resulted in a 2-log reduction of *P. aeruginosa* with gentamicin and has disrupted biofilm integrity through thermal degradation and cyclic di-GMP signaling, leading to bacterial dispersion [36]. Several nano compounds exhibit potent antimicrobial activity against various microorganisms. For instance, copper nanoparticles have been reported to disrupt bacterial cytoplasmic membranes, with high concentrations leading to the coagulation of biofilm-forming bacterial proteins. These effects have been shown to inhibit the growth of *S. aureus* and *P. aeruginosa* [37].

3.6 Effect of nano-iron on blood coagulation factors: PTT and PT

Figure 6 illustrates the in vitro effect of nano-iron synthesized from Arabic gum extract on PTT, which is a crucial indicator of both intrinsic and common coagulation pathways, where prolonged clotting time suggests anticoagulant activity. The results demonstrate a concentration-dependent increase in PTT, indicating that nano-iron influences coagulation kinetics.

At low concentrations (<50 µg/mL), PTT exhibits a slight increase compared to the control group. The clotting time remains within a moderate range, suggesting a subtle effect of nano-iron in delaying coagulation at these doses. A significant prolongation in clotting time is observed at 50 µg/mL, which further increases at 100 µg/mL. The highest concentration (100 µg/mL) results in the most pronounced delay in coagulation, indicating a strong anticoagulant effect at elevated doses. In the control group, clotting time is higher than at low nano-iron concentrations (2-10 µg/mL) but lower than at high concentrations (50-100 µg/mL). This suggests that nano-iron may exhibit an inhibitory effect on coagulation, which intensifies with increasing dosage.

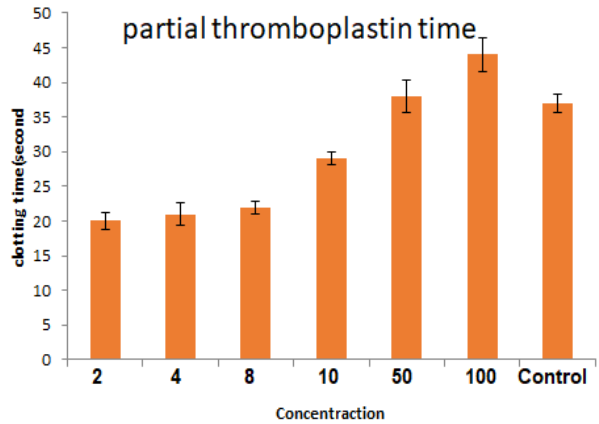

Figure 6. The effect of nano iron (FeNPs) on PTT clotting agent (unit: µg/mL)

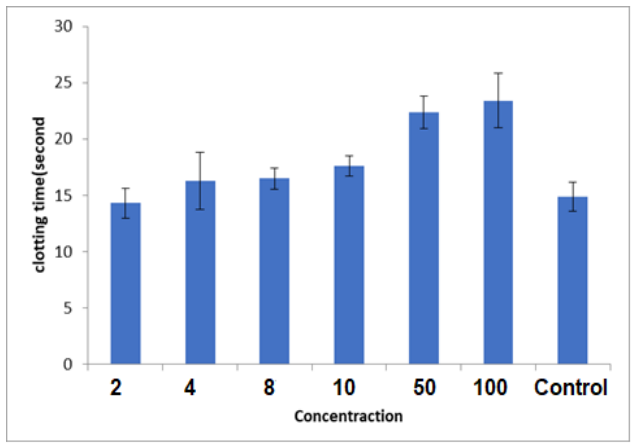

Figure 7. The effect of nano iron (FeNPs) on PT coagulation factor (unit: µg/mL)

Figure 7 illustrates the effect of nano iron on prothrombin time (PT), a key indicator for assessing the intrinsic and general pathways of blood coagulation. An increase in PT indicates a delay in blood clotting, indicating anticoagulant activity. At low concentrations (2-10 mg/mL), PT is moderately elevated compared to the control group, indicating

that lower doses of nano iron interfere with coagulation. However, this increased level is not greater at low doses, indicating that there is little or no dose-response at which the normal regulation of blood coagulation is altered. On the other hand, there is a concentration-dependent increase in blood coagulation after administration of nano-iron preparation. At 50 mg/mL, a sharp increase in PT was observed, which reached its maximum at 100 mg/mL. There is a direct relationship between concentration and the ability to reduce blood clotting, so it can act as an anti-clotting agent. This phenomenon indicates that the middle range of coagulation has a high anticoagulant property, with the above dose range showing great anticoagulant potential. The control sample had the lowest actual clotting time, indicating the coexistence of blood plasma and its strong clotting ability. While the samples treated with iron nanoparticles had a higher average clotting time, especially at higher-than-average concentrations, which increased the degree of their anticoagulant effect.

Blood clotting involves intrinsic pathways, with the intrinsic pathway activated by trauma and interactions between prekallikrein, high-molecular-weight kininogen, and factor XII with collagen in the endothelium and extrinsic and common clotting factors. The extrinsic pathway is stimulated by tissue injury, resulting in the release of tissue factor into the bloodstream [38]. The two pathways converge in a common and similar way, beginning with the generation of factor Xa and leading to the conversion of prothrombin to thrombin. Thrombin then converts fibrinogen to fibrin, forming a blood clot. Genetic and environmental disruptions can alter normal coagulation, leading to abnormal clot formation, a pathological condition known as thrombosis, which poses cardiovascular and cerebrovascular risks [39].

Nano-iron may interfere with coagulation factors such as factor VIII, IX, or XI, resulting in delayed thrombin formation. Additionally, it generates reactive oxygen species (ROS), which can modulate platelet function and fibrin formation. Nano-iron coated with Arabic gum may interact with plasma proteins, altering their function and reducing coagulation efficiency. The observed PTT prolongation suggests that nano-iron could have potential anticoagulant applications, particularly in conditions requiring clot prevention [40]. While low doses exhibit moderate effects, high doses may pose bleeding risks, necessitating careful dose optimization. The results indicate that nano-iron derived from Arabic gum exerts a dose-dependent anticoagulant effect, with higher concentrations significantly delaying clot formation. These findings highlight its potential as a blood-thinning agent, emphasizing the need for further research to assess its safety and clinical efficacy.

Trivalent nano-iron (Fe^{3+}) disrupts coagulation by interacting with clotting factors and altering fibrin structure, thereby delaying thrombin formation. Nano-iron and its hydrolyzed species adsorb coagulation factors such as factor VIII, IX, and XI, reducing their bioavailability in plasma [41, 42]. For instance, nano-iron inhibits factor Xa-mediated prothrombin conversion, a critical step in thrombin generation. Hydrolyzed nano-iron species impair factor XIII activity, destabilizing fibrin clots and promoting early fibrinolysis [43, 44]. Fe^{3+} binds to serine proteases (e.g., thrombin and factor Xa), reversibly inhibiting their amidolytic activity, thereby delaying fibrinogen-to-fibrin conversion [45], additionally, Fe^{3+} modifies fibrinogen/fibrin interactions, leading to denser, interwoven fibrin fibers with spherical aggregates instead of the natural mesh-like structure. This altered fibrin is mechanically weaker and more prone to degradation. Over time, $FeCl_3$ solutions generate reactive radicals and hydrolytic species (e.g., $Fe(OH)^{2+}$ and $Fe_2(OH)_2^{4+}$), further extending clotting time. Aged $FeCl_3$ solutions exhibit an even more pronounced delay in coagulation [46]. Furthermore, Fe_3O_4 nanoparticles, when magnetically localized, can prevent systemic thrombin inhibition. Without targeted application, these nanoparticles reduce thrombin generation potential [47]. Collectively, these mechanisms delay thrombin formation and destabilize blood clots, demonstrating the dual role of iron as both a procoagulant (at high localized concentrations) and an anticoagulant (at systemic levels). Additionally, α-Fe_2O_3 nanoparticles have been shown to activate innate immune responses in human whole-blood models. Protein corona formation on these nanoparticles triggers contact system proteins, leading to strong activation of both the kallikrein-kinin system and coagulation pathways, even at low concentrations, accompanied by platelet consumption. These findings emphasize the complex and concentration-dependent effects of nano-iron on coagulation, suggesting its potential biomedical applications while highlighting the need for precise dose regulation to mitigate bleeding risks.

3.9 The effect of nano-iron on wound healing

Figure 8 shows the rate of wound contraction in embryonic fibroblast cells of mice after 72 hours of treatment with nano iron; the symmetry of the results between the treated and non-treated groups shows the existence of a significant difference in wound closure rates. The treated group showed a significantly higher rate of scratch shrinkage (~88%) compared to the untreated group (~78%), indicating that nano-iron promotes cell migration and wound closure efficiency, which is extremely important for tissue regeneration and repair. It is easy to close the wound, and nano-sized iron particles stimulate mild oxidative stress and can stimulate, at controlled levels, redox-sensitive signal pathways (for example, MAPK and PI3K/Akt) that regulate cell migration and proliferation [48, 49].

Iron is an essential component in many enzymes such as hydroxylase and oxygenase, which contribute to collagen synthesis and tissue regeneration, and the low rate of contraction in the untreated group is attributed to the slow natural healing process of the wound, which is likely to be limited due to the proliferation of fibroblasts and suboptimal migrations. This confirms the potential of nano-iron as a pro-regenerative agent, which may lead to the acceleration of tissue repair mechanisms. The results indicate that nano-sized iron can be explored as a therapeutic agent for wound healing applications, especially in chronic wounds or tissue injuries, and it is important to investigate dose-dependent effects, as excessive exposure to iron may lead to cellular toxicity and oxidative damage [50-52], and the data indicate that the nano-iron significantly enhances the closure of the scratches by the fibroblasts and possibly due to the period of cell proliferation, migration, and enzyme activation.

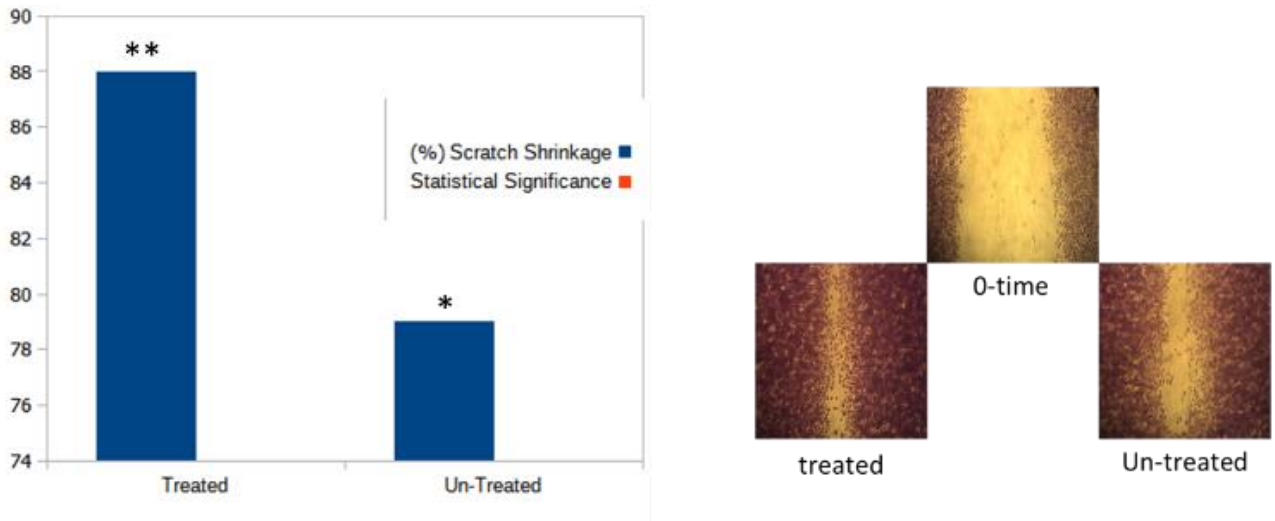

Figure 8. Shrinkage rate of the REF cell line treated with nano iron at a concentration of 50 mg/mL and the control of all the experimental cell groups after 72 hours of treatment (LSD1% = 3.761)

Composite nanomaterials have shown great potential in enhancing wound healing processes by accelerating tissue regeneration, reducing the risk of infection, and improving therapeutic outcomes. Aqueous emulsions loaded with nanoparticles provide a moist environment conducive to healing and possess natural healing properties such as excellent water absorption. Some composite nanomaterials can even increase angiogenesis, which promotes better wound healing. This is related to reducing oxidative stress that occurs during cell damage. Superoxide (O−) is a harmful byproduct of the mitochondrial trap, especially in the first two components of the electron transport chain (ETC), where electrons leak out. It is also produced by the enzyme NADPH oxidase in cells. Research on microorganisms is limited [53], and gold nanoparticles can accelerate wound healing. and repair damaged collagen tissues, and silver nanoparticles block respiratory enzyme pathways, modify microbial DNA and cell walls, and stimulate gold nanoparticles to release proteins necessary for wound healing and appearance. Anti-inflammatory and anti-platelet aggregation effects on blood vessels. The nanocomposites can mimic the environment of the extracellular matrix (ECM) of the wound, which facilitates better wound healing [54]. Studies have shown that nanocomposite treatments, especially AgNP-hydrogel compounds, accelerate wound healing without negative effects compared to control groups, and these nanocomposites show an active antibacterial activity against gram-negative and gram-positive bacteria while maintaining biocompatibility [55], and nanocomposites are a promising approach for wound healing through the combination of antibacterial properties and compatibility. The bioactivity and the ability to mimic natural tissue environments, which leads to faster and more effective wound repair, help the nanomaterials because they help in the migration and diffusion of the fibroblasts used in the scratch test [56]. Stimulating cells through reducing the factors that delay the success of wound healing, such as cytokines that cause inflammation in addition to oxidative stress, and the appearance of hydrogels modified with nanoparticles have very promising potential in the field of wound healing, thanks to their ability to accelerate tissue regeneration, reduce the risk of infection, and facilitate improved therapeutic results [57, 58].

4. CONCLUSION

This study highlights the biomedical potential of iron nanoparticles (FeNPs) synthesized from gum Arabic; the trial results demonstrated the future multifunctional potential of iron oxide nanoparticles. They exhibited significant antibacterial and anti-inflammatory activity (e.g., 91% membrane stabilization), anticoagulant effects comparable to those of an anticoagulant (clot dissolution within 16 minutes), and enhanced wound healing via fibroblast proliferation. These findings highlight the need for further research to evaluate toxicity, clinical feasibility, and long-term efficacy to develop their biomedical applications.

ACKNOWLEDGMENTS

The first author would like to thank the Deanship of the College of Education for Women, University of Anbar, Iraq, for providing all research materials and facilitating the completion of the study.

REFERENCES

[1] Khan, W.S., Asmatulu, E., Asmatulu, R. (2025). Nanotechnology emerging trends, markets and concerns. In Nanotechnology Safety, pp. 1-21. https://doi.org/10.1016/B978-0-443-15904-6.00017-4

[2] Kumar, P., Thakur, N., Kumar, K., Kumar, S., Dutt, A., Thakur, V.K., Gutiérrez-Rodelo, C., Thaku, P., Navarrete, A., Thakur, N. (2024). Catalyzing innovation: Exploring iron oxide nanoparticles-origins, advancements, and future application horizons. Coordination Chemistry Reviews, 507: 215750. https://doi.org/10.1016/j.ccr.2024.215750

[3] Ashour, M.A., Fatima, W., Imran, M., Ghoneim, M.M., Alshehri, S., Shakeel, F. (2022). A review on the main phytoconstituents, traditional uses, inventions, and patent literature of gum Arabic 1 emphasizing *Acacia seyal*. Molecules, 27(4): 1171. https://doi.org/10.3390/molecules27041171

[4] Aldhalemi, M.A., Shanshool, A.J., Taha, A.A. (2024).

Enhancing enzymatic activity through co-immobilization of protease and lipase enzymes on magnetic nano-iron oxides coated with gum Arabic. IOP Conference Series: Earth and Environmental Science, 1371(6): 062046. https://doi.org/10.1088/1755-1315/1371/6/062046

[5] Manimaran, K., Yanto, D.H.Y., Govindasamy, M., Karunanithi, B., Alasmary, F.A., Habab, R.A. (2024). Biological synthesis and characterization of iron oxide (FeO) nanoparticles using Pleurotus citrinopileatus extract and its biomedical applications. Biomass Conversion and Biorefinery, 14(11): 12575-12585. https://doi.org/10.1007/s13399-023-04382-8

[6] Meng, Y.Q., Shi, Y.N., Zhu, Y.P., Liu, Y.Q., et al. (2024). Recent trends in preparation and biomedical applications of iron oxide nanoparticles. Journal of Nanobiotechnology, 22(1): 24. https://doi.org/10.1186/s12951-023-02235-0

[7] Meletis, G., Skoura, L., Protonotariou, E. (2024). Antimicrobial resistance and antimicrobial therapy of clinically relevant bacteria. Antibiotics, 13(8): 691. https://doi.org/10.3390/antibiotics13080691

[8] Loganathan, S., Govindasamy, M., Habila, M.A., Manimaran, K. (2023). Green synthesis of iron oxide nanoparticles using *Pterolobium hexapetalum* (roth) santapau & wagh leaves extract and their biological applications. Biocatalysis and Agricultural Biotechnology, 54: 102905. https://doi.org/10.1016/j.bcab.2023.102905

[9] Salehirozveh, M., Dehghani, P., Mijakovic, I. (2024). Synthesis, functionalization, and biomedical applications of iron oxide nanoparticles (IONPs). Journal of Functional Biomaterials, 15(11): 340. https://doi.org/10.3390/jfb15110340

[10] Montiel Schneider, M.G., Martín, M.J., Otarola, J., Vakarelska, E., Simeonov, V., Lassalle, V., Nedyalkova, M. (2022). Biomedical applications of iron oxide nanoparticles: Current insights progress and perspectives. Pharmaceutics, 14(1): 204. https://doi.org/10.3390/pharmaceutics14010204

[11] Luktuke, S., Raj, A., Santra, S., Das, S., et al. (2024). Interaction of Fe_2O_3 and Fe_3O_4 nanoparticle with pathogenic bacteria: A in-silico molecular mechanism study. Nanoscience & Nanotechnology-Asia, 14(1). https://doi.org/10.2174/0122106812286623240125130324

[12] Vernet-Crua, A., Cruz, D.M., Mostafavi, E., Truong, L.B., Barabadi, H., Cholula-Díaz, J.L., Guisbiers, G., Webster, T.J. (2023). Green-synthesized metallic nanoparticles for antimicrobial applications. In Nanomedicine, pp. 297-338. https://doi.org/10.1016/B978-0-12-818627-5.00014-2

[13] Harandi, F.N., Khorasani, A.C., Shojaosadati, S.A., Hashemi-Najafabadi, S. (2022). Surface modification of electrospun wound dressing material by Fe_2O_3 nanoparticles incorporating Lactobacillus strains for enhanced antimicrobial and antibiofilm activity. Surfaces and Interfaces, 28: 101592. https://doi.org/10.1016/j.surfin.2021.101592

[14] Samokhin, Y., Varava, Y., Diedkova, K., Yanko, I., et al. (2025). Electrospun chitosan/polylactic acid nanofibers with silver nanoparticles: Structure, antibacterial, and cytotoxic properties. ACS Applied Bio Materials, 8(2): 1027-1037. https://doi.org/10.1021/acsabm.4c01252

[15] Ebrahimi, S.R., Nikbakht, M., Abadi, M.S.S., Gholipour, A., Bagheri, M., Validi, M. (2025). Investigation of biocompatibility and antibacterial properties of electrospun chitosan/polyethylene oxide-based scaffolds containing propolis extract against *Enterococcus faecalis*, *Pseudomonas aeruginosa*, *Staphylococcus aureus* and *Staphylococcus epidermidis*. Heliyon, 11(3): e42228. https://doi.org/10.1016/j.heliyon.2025.e42228

[16] Tiwari, A.K., Pandey, P.C., Gupta, M.K., Narayan, R.J. (2025). Nano–bio interaction and antibacterial mechanism of engineered metal nanoparticles: fundamentals and current understanding. Journal of Cluster Science, 36(1): 1-33. https://doi.org/10.1007/s10876-024-02728-4

[17] Bharathy, P., Thanikachalam, P.V., Jayaprakash, S., Dowlath, P., Madhaiyan, P. (2025). Biosynthesis and characterization of *Ixora coccinea*-based iron oxide nanoparticles: Potential applications in wound healing and therapeutics. Biomedical Materials & Devices, 1-13. https://doi.org/10.1007/s44174-024-00271-4

[18] Tu, Y., Li, Y., Qu, G., Ning, Y., Li, B., Li, G., Wu, M., Li, S.J., Huang, Y.G. (2025). A Review of basic fibroblast growth factor delivery strategies and applications in regenerative medicine. Journal of Biomedical Materials Research Part A, 113(1): e37834. https://doi.org/10.1002/jbm.a.37834

[19] Shanmugam, R., Anandan, J., Abalkhail, T., Alqahtani, A.M., Roy, A. (2025). Green synthesis of iron oxide nanoparticles using *Cissus rotundifolia* and its antibacterial activity against wound pathogens. Journal of the Indian Chemical Society, 102(3): 101599. https://doi.org/10.1016/j.jics.2025.101599

[20] Świerczyńska, M., Król, P., Hernández Vázquez, C. I., Piekarska, K., Woźniak, K., Juszczak, M., Mrozińska, Z., Kudzin, M.H. (2024). Blood coagulation activities and influence on DNA condition of alginate—Calcium composites prepared by freeze-drying technique. Marine Drugs, 22(9): 415. https://doi.org/10.3390/md22090415

[21] Ali, A., Zafar, H., Zia, M., ul Haq, I., Phull, A.R., Ali, J.S., Hussain, A. (2016). Synthesis, characterization, applications, and challenges of iron oxide nanoparticles. Nanotechnology, Science and Applications, 9: 49-67. https://doi.org/10.2147/NSA.S99986

[22] Zhou, W., Apkarian, R., Wang, Z.L., Joy, D. (2007). Fundamentals of scanning electron microscopy (SEM). In Scanning Microscopy for Nanotechnology: Techniques and Applications, pp. 1-40. https://doi.org/10.1007/978-0-387-39620-0_1

[23] Cervini-Silva, J., Camacho, A.N., Palacios, E., del Angel, P., et al. (2016). Anti-inflammatory, antibacterial, and cytotoxic activity by natural matrices of nano-iron (hydr) oxide/halloysite. Applied Clay Science, 120: 101-110. https://doi.org/10.1016/j.clay.2015.10.004

[24] Simak, J., De Paoli, S. (2017). The effects of nanomaterials on blood coagulation in hemostasis and thrombosis. Wires Nanomedicine and Nanobiotechnology, 9(5): e1448. https://doi.org/10.1002/wnan.1448

[25] Ilinskaya, A.N., Dobrovolskaia, M.A. (2013). Nanoparticles and the blood coagulation system. Part II: Safety concerns. Nanomedicine, 8(6): 969-981. https://doi.org/10.2217/nnm.13.49

[26] Haghniaz, R., Rabbani, A., Vajhadin, F., Khan, T., et al. (2021). Anti-bacterial and wound healing-promoting

effects of zinc ferrite nanoparticles. Journal of Nanobiotechnology, 19: 1-15. https://doi.org/10.1186/s12951-021-00776-w

[27] Li, Y., Cheng, Y.F. (2018). Photocatalytic anti-bioadhesion and bacterial deactivation on nanostructured iron oxide films. Journal of Materials Chemistry B, 10: 11506. https://doi.org/10.1039/C8NR03684E

[28] Borcherding, J., Baltrusaitis, J., Chen, H., Stebounova, L., Wu, C.M., Rubasinghege, G., Mudunkotuwa, I.A., Caraballo, J.C., Zabner, J., Grassian, V.H., Comellas, A.P. (2014). Iron oxide nanoparticles induce Pseudomonas aeruginosa growth, induce biofilm formation, and inhibit antimicrobial peptide function. Environmental Science: Nano, 110: 87. https://doi.org/10.1039/C3EN00029J

[29] Yasmeen, F., Parveen, R., Fatima, H., Arooj, N., Sarwar, I., Iqbal, M. (2024). Nano iron with macro applications. Transactions of the Indian National Academy of Engineering, 9: 725-736. https://doi.org/10.1007/s41403-024-00484-5

[30] Liang, E., Xu, L., Su, J., Yang, Y., Liu, Y. (2023). Nano iron tetroxide-modified rice husk biochar promoted Feammox performance of *Klebsiella* sp. FC61 and synergistically removed Ni^{2+} and ciprofloxacin. Bioresource Technology, 382: 129183. https://doi.org/10.1016/j.biortech.2023.129183

[31] Namasivayam, S.K.R., Samrat, K., R.S., A.B., Kavisri, M., Kennedy, J.F., Moovendhan, M. (2024). Pectin-nano zero valent iron nanocomposites for efficient heavy metal removal and bactericidal action against waterborne pathogens—innovative green solution towards environmental sustainability. International Journal of Biological Macromolecules, 277: 133990. https://doi.org/10.1016/j.ijbiomac.2024.133990

[32] Shen, X., Ma, R., Huang, Y., Chen, L., et al. (2020). Nano-decocted ferrous polysulfide coordinates ferroptosis-like death in bacteria for anti-infection therapy. Nano Today, 35: 100981. https://doi.org/10.1016/j.nantod.2020.100981

[33] Cao, Y.H., Cai, W.J., He, X.W., Song, H.L., Gao, J.S., Yang, Y.L., Zhou, J.F. (2024). A review of advances & potential of applying nanomaterials for biofilm inhibition. Npj Clean Water, 7: 131. https://doi.org/10.1038/s41545-024-00423-5

[34] Mohanta, Y.K., Chakrabartty, I., Mishra, A K., Chopra, H., et al. (2023). Nanotechnology in combating biofilm: A smart and promising therapeutic strategy. Frontiers in Microbiology, 13: 1028086. https://doi.org/10.3389/fmicb.2022.1028086

[35] Liu, H., Xing, F., Yu, P., Zhe, M., Shakya, S., Liu, M., Xiang, Z., Duan, X., Ritz, U. (2024). Multifunctional aerogel: A unique and advanced biomaterial for tissue regeneration and repair. Materials & Design, 243: 113091. https://doi.org/10.1016/j.matdes.2024.113091

[36] He, X., Dai, L., Ye, L., Sun, X., Enoch, O., Hu, R., Zan, X., Lin, F., Shen, J. (2022). A vehicle-free antimicrobial polymer hybrid gold nanoparticle as synergistically therapeutic platforms for Staphylococcus aureus infected wound healing. Advanced Science, 9(14): 2105223. https://doi.org/10.1002/advs.202105223

[37] Arunachalam, K., Pandurangan, P., Shi, C., Lagoa, R. (2023). Regulation of *Staphylococcus aureus* virulence and application of nanotherapeutics to eradicate *S. aureus* infection. Pharmaceutics, *15*(2): 10. https://doi.org/10.3390/pharmaceutics15020310

[38] Granados-Carrera, C.M., Castro-Criado, D., Abdullah, J. A.A., Jiménez-Rosado, M., Perez-Puyana, V.M. (2025). Aerogels based on chitosan and collagen modified with Fe_2O_3 and Fe_3O_4 nanoparticles: Fabrication and characterization. Polymers, 17(2): 133. https://doi.org/10.3390/polym17020133

[39] Tran, H.D., Moonshi, S.S., Xu, Z.P., Ta, H.T. (2022). Influence of nanoparticles on the haemostatic balance: Between thrombosis and haemorrhage. Biomaterials Science, 10(1): 10-50. https://doi.org/10.1039/D1BM01351C

[40] Kottana, R.K., Maurizi, L., Schnoor, B., Morris, K., Webb, J.A., Massiah, M.A., Millot, N., Papa, A.L. (2021). Anti-platelet effect induced by iron oxide nanoparticles: Correlation with conformational change in fibrinogen. Small, 17(1): 2004945. https://doi.org/10.1002/smll.202004945

[41] Shi, Z., Lan, G., Hu, E., Lu, F., Qian, P., Liu, J., Dai, F., Xie, R. (2022). Targeted delivery of hemostats to complex bleeding wounds with magnetic guidance for instant hemostasis. Chemical Engineering Journal, 427: 130916. https://doi.org/10.1016/j.cej.2021.130916

[42] Yenurkar, D., Choudhary, A., Shrivastava, A., Pragya, P., et al. (2024). Potassium ferric oxalate nanoparticles prevent human blood clotting and thrombosis in a mouse model. BioRxiv. https://doi.org/10.1101/2024.11.04.621820

[43] Fithri, N.A., Wu, Y., Cowin, G., Akther, F., Tran, H.D., et al. (2023). Gold-iron oxide nanoparticle: A unique multimodal theranostic approach for thrombosis. Applied Materials Today, 31: 101750. https://doi.org/10.1016/j.apmt.2023.101750

[44] Samridhi, Setia, A., Mehata, A.K., Priya, V., Pradhan, A., Prasanna, P., Mohan, S., Muthu, M.S. (2024). Nanoparticles for thrombus diagnosis and therapy: emerging trends in thrombus-theranostics. Nanotheranostics, 8(2): 127. https://doi.org/10.7150/ntno.92184

[45] Zhang, B., Fan, K. (2025). Design and application of ferritin-based nanomedicine for targeted cancer therapy. Nanomedicine, 481-500. https://doi.org/10.1080/17435889.2025.2459056

[46] Santana-Otero, A., Harper, A., Telling, N., Ortega, D., Cabrera, D. (2024). Magnetic coagulometry: towards a new nanotechnological tool for ex vivo monitoring coagulation in human whole blood. Nanoscale, 16(7): 3534-3548. https://doi.org/10.1039/D3NR02593D

[47] Zhao, W., Liu, Q., Zhang, X., Su, B., Zhao, C. (2018). Rationally designed magnetic nanoparticles as anticoagulants for blood purification. Colloids and Surfaces B: Biointerfaces, 164: 316-323. https://doi.org/10.1016/j.colsurfb.2018.01.050

[48] Shi, X., Pu, H., Shi, L.L., He, T.C., Chen, J. (2025). Additive manufacturing technologies and translation of transistor-based point-of-care (POC) biosensors from laboratory to real-life applications. Nanoscale, 17(16): 9804-9833. https://doi.org/10.1039/D4NR04441J

[49] Fröhlich, E. (2016). Action of nanoparticles on platelet activation and plasmatic coagulation. Current Medicinal Chemistry, 23(5): 408-430. https://doi.org/10.2174/0929867323666160106151428

[50] Li, Y., Tan, Y., Zhao, H., Chen, S., Nilghaz, A., Cao, R., Zhou, S. (2025). Green biosynthetic silver nanoparticles

from *Ageratum conyzoides* as multifunctional hemostatic agents: Combining hemostasis, antibacterial, and anti-inflammatory properties for effective wound healing. Materials Today Bio, 31: 101468. https://doi.org/10.1016/j.mtbio.2025.101468

[51] Mrozińska, Z., Świerczyńska, M., Juszczak, M., Woźniak, K., Kudzin, M.H. (2025). Evaluation of antimicrobial activity, hemostatic efficacy, blood coagulation dynamics, and DNA damage of linen–copper composite materials. Journal of Composites Science, 9(1): 30. https://doi.org/10.3390/jcs9010030

[52] Chen, Y., Hou, S. (2023). Recent progress in the effect of magnetic iron oxide nanoparticles on cells and extracellular vesicles. Cell Death Discovery, 9: 195. https://doi.org/10.1038/s41420-023-01490-2

[53] Han, G., Nguyen, L.N., Macherla, C., Chi, Y., Friedman, J.M., Nosanchuk, J.D., Martinez, L.R. (2012). Nitric oxide-releasing nanoparticles accelerate wound healing by promoting fibroblast migration and collagen deposition. Cell Injury, Repair, Aging, and Apoptosis, 180(4): 1465-1473. https://doi.org/10.1016/j.ajpath.2011.12.013

[54] Frank, S., Kämpfer, H., Wetzler, C., Pfeilschifter, J. (2002). Nitric oxide drives skin repair: Novel functions of an established mediator. The American Journal of Pathology, 61(3): 882-888. https://doi.org/10.1046/j.1523-1755.2002.00237.x

[55] Huang, L., Guo, Z., Yang, X., Zhang, Y., Liang, Y., Chen, X., Qiu, X., Chen, X. (2025). Advancements in GelMA bioactive hydrogels: Strategies for infection control and bone tissue regeneration. Theranostics, 15(2): 460-493. https://doi.org/10.7150/thno.103725

[56] Kılıç, H., Ceylan, D. (2025). Multi-responsive shape memory and self-healing hydrogels with gold and silver nanoparticles. Journal of Materials Chemistry B, 13(1): 336-353. https://doi.org/10.1039/D4TB01720J

[57] Alissa, M., Alghamdi, A., Alshehri, M.A. (2025). Curcumin nanoparticles loaded in a bioengineering and biodegradable silk-hyaluronan scaffold triggered wound healing by regulating inflammation and accelerating proliferation in a diabetic rat model. Tissue and Cell, 95: 102840. https://doi.org/10.1016/j.tice.2025.102840

[58] Wang, J., Liu, H., Liu, M., Shen, T., Wen, T., He, F., Wang, X. (2025). A dual gene-activated dermal scaffolds loaded with nanocomposite particles expressing of VEGF and aFGF: Promoting wound healing by early vascularization. International Journal of Biological Macromolecules, 307: 141831. https://doi.org/10.1016/j.ijbiomac.2025.141831